Development of a Novel Axial Blood Pump With a Thrust Force Levitation Technology—Device Design and Levitation Experiments

Ryota Magari and Wataru Hijikata, *Member, IEEE*

***Abstract*—The durability of a blood pump has been enhanced owing to the development of noncontact bearings. However, hydrodynamic bearings exhibit a risk of blood trauma owing to their narrow gaps, and magnetic bearings exhibit a risk of malfunctioning of their active control system. Therefore, in this study, we developed a blood pump that can levitate an impeller with a large gap without any active control system. In the proposed system, the impeller is levitated using a combination of the thrust force and permanent magnets. The thrust force, which is generated on the impeller as a reaction force to pump blood, changes based on the interaction between the housing geometry and impeller position. By utilizing this characteristic, the thrust force acted as a passive restoring force. A pump prototype was fabricated to verify the levitation. The experimental results showed that the impeller can be passively levitated in the axial direction by balancing the thrust and magnetic force with a gap of as low as 500 μm without active control. The pump head was 33.8 mmHg at 10 000 r/min and 1.5 L/min. The proposed principle is expected to contribute to the development of a blood pump with lower blood trauma and higher reliability.**

***Index Terms*—Axial blood pump, levitation system, noncontact bearing, thrust force, ventricular assist device (VAD).**

I. Introduction

HEART transplantation is a treatment option for patients with serious heart diseases, such as dilated cardiomyopathy. However, the number of patients waiting for transplantation is much higher than that of donors [1]. Therefore, ventricular assist devices (VADs) have been used as a bridge to transplants (BTTs). VADs are classified into two types: extracorporeal and implantable. Extracorporeal VADs are placed outside the body of a patient [2], [3], [4], [5], [6], [7]. Although the pump is large and the movement of the patient is limited, this type of pump head can be detached for cost-effective use. Implantable VADs are placed inside a patient's body [8], [9], [10], [11], enabling patients to move freely. Implantable VADs are required to improve patients' quality of life.

Currently, VADs are considered not only as BTT but also as destination therapy (DT). In the United States, more than 70% of VADs were implanted as DT in 2019 [12]. To use VADs as DT, problems resulting from long-term use, such as thrombus formation and durability, must be solved. Methods for preventing thrombus formation and its detection have been proposed [13], [14], [15], [16].

Noncontact bearings have been used to increase the durability of VADs. There are two types of noncontact bearings: hydrodynamic bearings [17], [18] and active magnetic bearings [19], [20], [21], [23]. In a hydrodynamic bearing system, the impeller is suspended by fluid forces generated in thin blood films that separate the impeller and pump housing [24], [25]. This system does not require active control with sensors, and this contributes to system reliability. However, this type of bearing system can lead to severe blood trauma. Although red blood cells are approximately 8 μm in diameter, the blood film between the impeller and pump housing is only a few dozen micrometers in diameter. Therefore, high shear stress is applied to red blood cells, which leads to serious blood trauma.

In an active magnetic bearing system, the impeller is suspended by magnetic force. According to Earnshaw's theorem [26], levitation in all six degrees of freedom (DOFs) cannot be achieved using a static magnetic field and paramagnetic materials alone. At least 1-DOF for levitation requires feedback control using electromagnets, a force from a dynamic magnetic field, a force acting on diamagnetic materials, or other external forces. Therefore, active magnetic bearing systems use electromagnets and sensors to control the position of the impeller [27], [28], [29], [30]. A pump with this system can realize a larger fluid gap in the range of 200–300 μm, which contributes to a decrease in blood trauma. However, active feedback control using sensors and electromagnets has a high risk of pump failure because it cannot maintain impeller levitation if a part of the system fails.

Therefore, the objective of this study is to develop a VAD with a novel levitation system for an impeller with a large gap without active control. The large gap reduces shear stress on blood cells, which prevents blood trauma. Passive levitation eliminates the risk of sensor failure and contributes to the realization of system

Manuscript received 26 March 2022; revised 8 April 2023 and 4 June 2023; accepted 13 June 2023. This work was supported by JSPS KAKENHI under Grant JP20H02098 and Grant JP23H00157. Recommended by Technical Editor P. Yan and Senior Editor Y. Li. *(Corresponding author: Wataru Hijikata.)*

The authors are with the School of Engineering, Tokyo Institute of Technology, Tokyo 152-8550, Japan (e-mail: magari.r.aa@m.titech.ac.jp; hijikata.w.aa@m.titech.ac.jp).

Color versions of one or more figures in this article are available at https://doi.org/10.1109/TMECH.2023.3290970.

Digital Object Identifier 10.1109/TMECH.2023.3290970

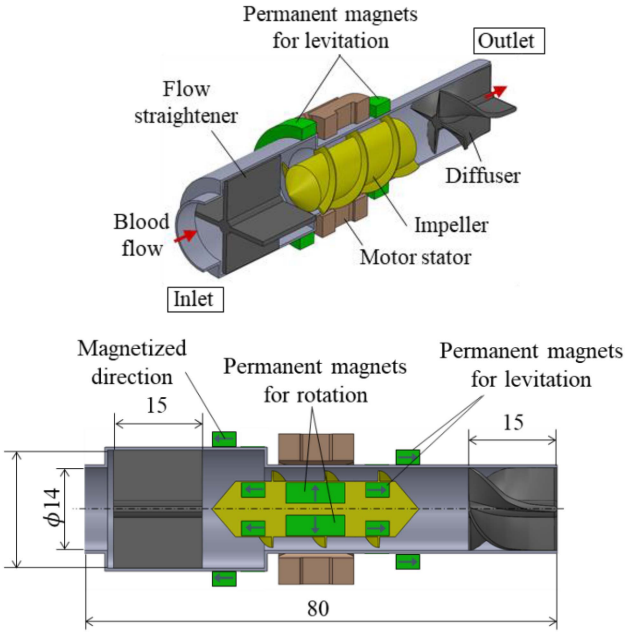

Fig. 1. Configuration of a proposed axial flow pump.

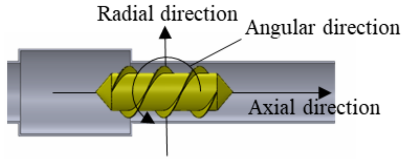

Fig. 2. Definition of a coordinate system for the force acting on the impeller and displacement of the impeller.

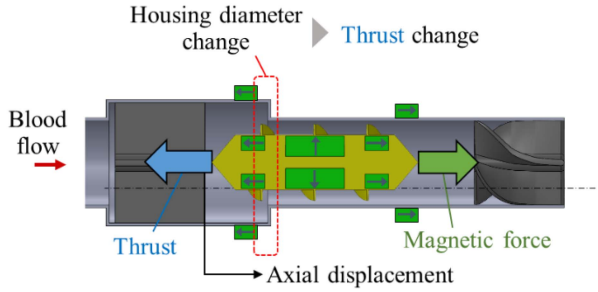

Fig. 3. Levitation principle in the axial direction.

reliability. In this study, thrust force levitation technology, which is a novel levitation system utilizing a combination of magnetic forces generated by permanent magnets and thrust generated by the rotation of the impeller, was proposed, and its feasibility was experimentally evaluated. The target dimensions of the proposed VAD were 80 mm in length and 20 mm in diameter with the smallest gap of 500 μm.

II. Principle of the Thrust Force Levitation Technology

A. Configuration of the Proposed Pump

The axial pump, as shown in Fig. 1, was adopted as the basic structure. The pump consisted of a housing, impeller, flow straightener, diffuser, direct-drive motor, and passive magnetic bearing. The housing used in the proposed pump has a unique shape. Specifically, its diameter is larger in the middle part of the pump. The flow straightener was installed on the inlet side to suppress turbulence and swirling flow. The diffuser installed at the outlet converts the swirling flow generated by the rotating impeller into a straight flow and increases the pump head. Stator coils and rotor magnets were installed outside the housing and inside the impeller, respectively. The coils are coreless not to generate a magnetic attractive force between them and the other magnets.

B. Overview of the Levitation Principle

In this study, the forces acting on the impeller and displacement of the impeller are considered in the coordinate system, as shown in Fig. 2. Although the radial and angular directions have 2-DOFs, only 1-DOF was considered because of its geometric symmetry. In the axial direction, the magnetic force and thrust act on the impeller, and levitation is realized by passively adjusting these forces. The thrust force acts on the impeller as a reaction force against blood flow generation. In the radial and angular directions, the impeller was supported by magnetic repulsion. The proposed levitation system, which supports 5-DOFs, except for rotation around the axial direction, is realized by satisfying conditions 1)–3) shown in the following text. In this study, positive stiffness indicates that the restoring force or torque acts against the displacement of the impeller.

1) *Axial direction:* An equilibrium point exists, and the resultant force of thrust and magnetic force exhibits a positive stiffness around it.
2) *Radial direction:* An equilibrium point exists, and the magnetic force exhibits a positive stiffness around it.
3) *Angular direction:* An equilibrium point exists, and the torque generated by the magnetic force exhibits a positive stiffness around it.

C. Levitation Principle in the Axial Direction

Fig. 3 shows the forces acting on the impeller in the axial direction. According to Earnshaw's law, it is impossible to levitate an impeller with only permanent magnets because the stiffness becomes negative for at least 1-DOF. Hence, electromagnets or other external forces are required for DOFs with a negative stiffness. In the proposed levitation system, the thrust force is utilized as an external force in the axial direction to levitate the impeller.

In the axial pump, the thrust T[N] acting on the impeller was theoretically calculated using the following equation [31]:

$$T = \gamma \frac{SH}{1-\mu^2}\left(1 - \frac{gH_{th}}{2u_2^2}\right). \quad (1)$$

where γ denotes the volume weight (kgf/m^3), S denotes the cross-sectional area of the flow path at the end of the impeller (m^2), H denotes the total pump head (m), μ denotes the ratio

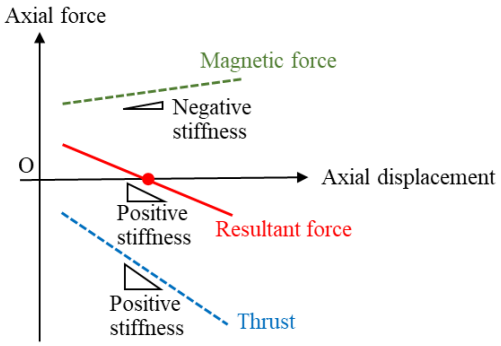

Fig. 4. Resultant force in the axial direction.

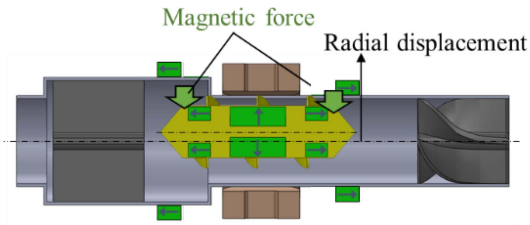

Fig. 5. Levitation principle in the radial direction.

of the axis to the diameter of the impeller, g denotes the gravitational acceleration (m/s^2), H_{th} denotes the theoretical pump head (m), and u_2 denotes the circumferential fluid speed (m/s). The total pump head H includes the energy loss through the pump, whereas the theoretical pump head H_{th} is calculated by ignoring the energy loss. According to (1), the thrust increases as the total pump head and cross-sectional area of the flow path at the end of the impeller increase. In addition, it has been reported that the pump head decreases as the gap between the housing and impeller increases [32]. This is due to the fact that a larger gap increases the backflow. By considering these characteristics, the proposed pump was designed to exhibit a positive stiffness in the thrust force against the displacement of the impeller.

As shown in Fig. 3, the diameter of the housing changes in the middle area, which causes a change in the cross-sectional area of the flow path, pump head, and gap between the housing and impeller when the impeller is displaced. As shown in Fig. 4, even if the stiffness of the magnetic force in the axial direction is negative, the resultant force of the magnetic force and thrust force can have a positive stiffness and an equilibrium point position.

D. Levitation Principle in the Radial and Angular Direction

As shown in Fig. 5, when the impeller moves in the radial direction, the repulsive force generated by the permanent magnets acts as a restoring force. In addition, as shown in Fig. 6, when the impeller moved in the angular direction, the magnetic force acted as a restoring torque. Consequently, the stiffness in the radial and angular directions was positive, and the impeller can maintain contactless levitation in these directions.

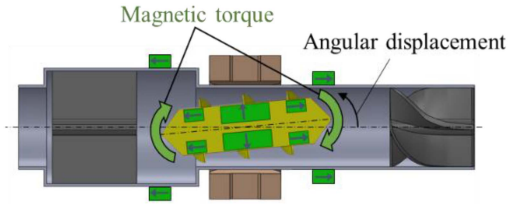

Fig. 6. Levitation principle in the angular direction.

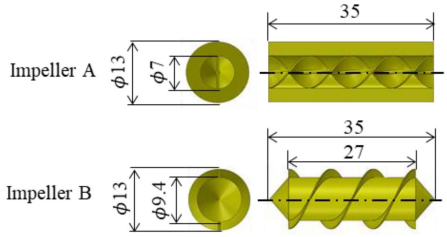

Fig. 7. Simulation models for impeller geometry.

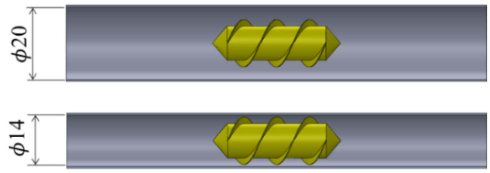

Fig. 8. Two circular pipes with different diameters for investigating the thrust force acting on the impeller and pump head in CFD analysis.

III. Numerical Analysis of Axial Thrust

A. Method

To realize the proposed system, the thrust force should exhibit a positive stiffness. Therefore, the pump was designed to exhibit this type of characteristic using computational fluid dynamics (CFD) analysis. ANSYS Fluent (ver19.0, ANSYS Japan, Tokyo, Japan) was used as the solver. Blood was assumed as an incompressible Newtonian fluid with a density of 1060 kg/m^3 and viscosity of 3.6 mPa · s. The boundary conditions were set as follows: inlet flow rate of 1.5 L/min and outlet gauge pressure of 0 Pa. The rotational speed of the impeller is 10 000 r/min. A realizable k–ε turbulence model was used for turbulence modeling. The factors that influence thrust are the rotational speed, shape of the impeller, straightener, diffuser, and housing. In this study, the shape of impeller was designed. The detailed design process is as follows.

1) Impellers A and B in Fig. 7 were placed in the two circular pipes, as shown in Fig. 8, and the thrust and pump head were calculated. Impeller A has spiral blades, and rotor magnets are installed on its outer shell. It was designed to increase the motor torque by reducing the gap between the coils and rotor magnets. Conversely, impeller B has a general shape for an axial flow pump, and rotor magnets are installed along its axis. The pump proposed in this study has a housing with a change in its diameter, flow straightener, and diffuser. However, the calculated cost tends to increase when all parts are considered in

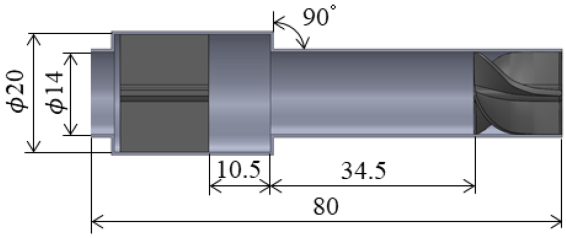

Fig. 9. Simulation model of housing with rapid change in its diameter.

TABLE I
RESULTS OF THE THRUST FORCE AND PUMP HEAD FOR TWO TYPES OF THE IMPELLERS IN CFD ANALYSIS

	Impeller A		Impeller B	
Flow path	ϕ20	ϕ14	ϕ20	ϕ14
Thrust	0.091 N	-0.20 N	-0.72 N	-0.93 N
Pressure	6.9 mmHg	5.8 mmHg	11 mmHg	42 mmHg

the CFD analysis. Therefore, as a first step, the thrust force and pump head were investigated using two circular pipes with different diameters (ϕ14 and ϕ20) without a straightener or diffuser. The basic design of the impeller was determined based on the analysis results.

2) In the next step, the impeller was installed in the housing with a straightener and diffuser, as shown in Fig. 9. The change in thrust was calculated by moving the impeller. Subsequently, the shape of the impeller was improved to increase the thrust changes.

B. Results

1) The simulation results of the thrust and pump head for the two types of impellers are shown in Table I. The positive direction was the same as that of the blood flow. Impellers A and B acquire a change in thrust based on the flow path diameter, and the changes were 0.29 N and 0.21 N, respectively. Therefore, both impellers can be used to realize the proposed system. The head pressure of impeller B is higher than that of impeller A. This was because the diameter of the blades of impeller A was smaller. Hence, the circumferential velocity decreased. Considering these results, it was determined that the blades should be placed outside the impeller.

1) Fig. 10 shows the simulation results of the thrust regarding the axial displacement z_{imp} of impeller B. The positive direction of the axial thrust was the same as that of blood flow. The position at which the impeller contacted the straightener is defined as $z_{\mathrm{imp}} = 0$. The results showed that the sensitivity of thrust to the displacement of the impeller was small. This is because the displacement of the impeller (< 5 mm) was too small when compared with the total length of the impeller blades (27 mm), and the flow path in the housing did not change significantly. Therefore, impeller C is designed, as shown in Fig. 11. Although impeller C has blades on the outside, similar to

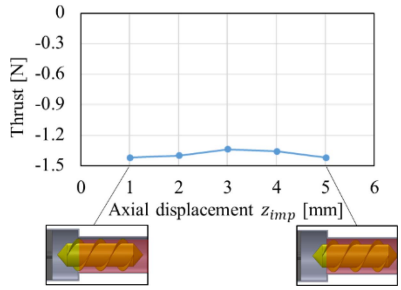

Fig. 10. Simulation results of thrust force with respect to the axial displacement of impeller B at 10 000 r/min and 1.5 L/min.

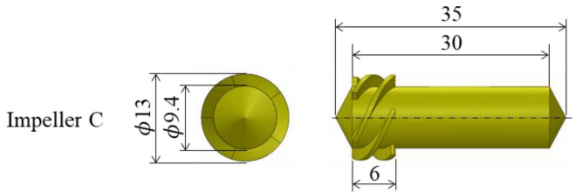

Fig. 11. Dimensions of impeller C.

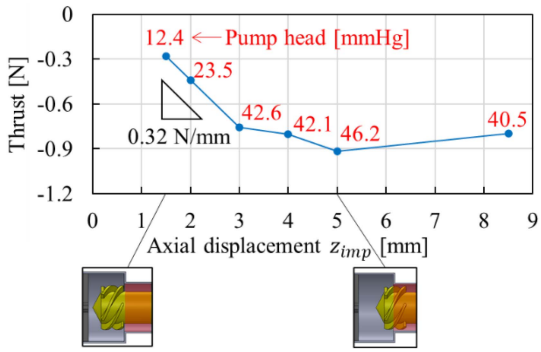

Fig. 12. Simulation results of thrust force and pump head with respect to the axial displacement of impeller C at 10 000 r/min and 1.5 L/min.

impeller B, the blade length of impeller C is shorter. This design is expected to have thrust sensitivity to impeller displacements of a few millimeters. To prevent a decrease in the pump head due to the shortening of the blades, the number of blades was increased from two to five. Fig. 12 shows the simulation results of the thrust and pump head with respect to the axial displacement of impeller C. The results showed that impeller C exhibited a high thrust sensitivity to the displacement. Its stiffness was 0.32 N/mm at position of 1.5 mm $\leq z_{\mathrm{imp}} \leq$ 3 mm. Therefore, impeller C was appropriate for the proposed system.

IV. NUMERICAL ANALYSIS OF MAGNETIC FORCE

To realize the proposed levitation system, passive magnetic bearings were designed considering the balance with thrust. The finite-element method-based 3-D magnetic-field analysis was performed using the ANSYS Maxwell software (ANSYS Japan, Tokyo). In this analysis, motor magnets and levitation magnets were modeled. Fig.13 shows the dimensions of the rotor magnets and magnetic bearing. The material corresponded

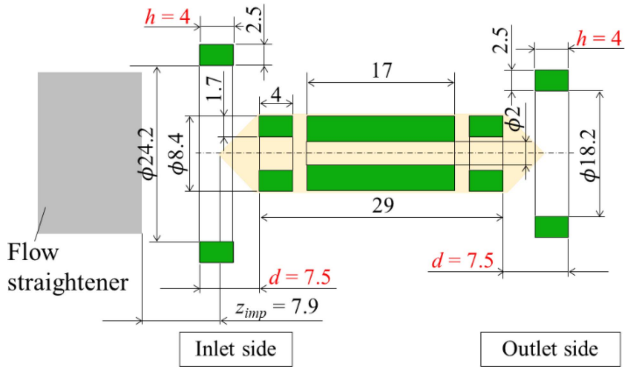

Fig. 13. Dimensions of permanent magnets.

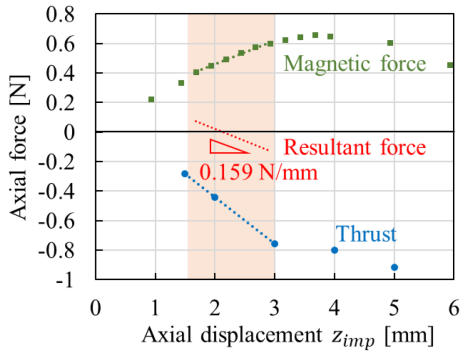

Fig. 14. Simulation results of magnetic force against the impeller position in the axial direction in the magnetic-field analysis. Resultant force was obtained from the axial magnetic force and thrust generated by impeller C with the housing having gradually change of its diameter at 10 000 r/min and 1.5 L/min.

to a neodymium magnet N35EH with a residual flux density of 1200 mT and coercivity of 868 kA/m.

Preliminary investigations have shown that the axial height h of a permanent magnet has a greater effect on its stiffness than its radial thickness. Therefore, h was used as the design variable and the radial thickness was fixed at 2.5 mm for the stator side and 1.7 mm for the impeller side by considering the strength of the permanent magnets and space limitations. The distance d between the permanent magnets is another parameter that has a significant effect on stiffness. Based on the above, a magnetic-field analysis was conducted for a total of 12 combinations of permanent magnet height h and distance d as design variables, $h = 3$, 4, 5 mm and $d = 5$, 7.5, 10, 12.5 mm, to determine the magnet dimensions that satisfy both levitation conditions 1)–3), as described in Section II-B and the following conditions.

1) The magnitude of the axial negative stiffness due to the permanent magnet must be 0.20 N/mm or less to ensure that it is smaller than the positive stiffness due to thrust (0.32 N/mm).
2) The positive stiffness in the radial and tilt directions should be as large as possible.

As a result, $h = 4$ mm and $d = 7.5$ mm were adopted.

Fig. 14 shows the simulation results for the axial magnetic force with respect to the impeller position and the resultant force obtained from the axial magnetic force and thrust. The linearized

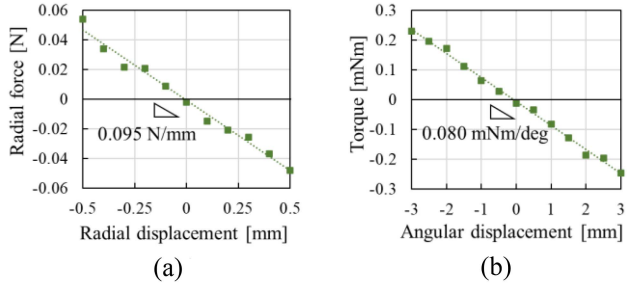

Fig. 15. Simulation results of magnetic force with respect to the impeller position in the radial and angular direction in the magnetic-field analysis. (a) Radial direction. (b) Angular direction.

curve was estimated using the least squares method. The stator permanent magnets were placed so that the thrust and magnetic force are balanced at $z_{\mathrm{imp}} = 2.1$ mm, where the positive stiffness of the thrust is at its maximum. As a result, Fig. 13 indicates the state with $z_{\mathrm{imp}} = 7.9$ mm. The resultant thrust and magnetic force exhibited a positive stiffness of 0.159 N/mm around this equilibrium point. These results satisfied the conditions of levitation in the axial direction, and the impeller was expected to levitate axially at around $z_{\mathrm{imp}} = 2.1$ mm.

Fig. 15 shows the simulation results of the radial and angular magnetic force with respect to the impeller position at the equilibrium point in the axial direction. Equilibrium points exist in both radial and angular directions, and the magnetic forces exhibit a positive stiffness of 0.095 N/mm and 0.080 mN·m/°, respectively.

These results satisfied the conditions of levitation in the radial and angular directions. The simulation results confirmed that the levitation conditions were satisfied in all the directions 1)–3), as described in Section II-B. Note that the diameter of the stator magnet ring on the outlet side is set to smaller than that on the inlet side to increase the stiffness in the radial and tilt directions. The difference in the inner diameters of these two rings may cause cross coupling between the radial and tilt motions. Although this is not considered in this study, if it will be a problem for levitation, aligning the diameters of the two rings can greatly reduce cross coupling.

V. Numerical Analysis of Motor Torque

The current density of the motor coils, required to rotate the impeller, was calculated using magnetic-field analysis. If an iron core is used in this pump, a magnetic attractive force is generated between the rotor magnet and core, resulting in negative stiffness in the radial and angular directions. Therefore, a coreless motor was used in this study. The required motor torque was set to 4.4 mN·m, which was obtained from the results of the CFD analysis with a rotational speed of 10 000 r/min, flow rate of 1.5 L/min, and head pressure of 23.5 mmHg, as conducted in Section III. Fig. 16 shows the configuration of the motor. The motor magnet had four poles. The motor was a three-phase motor (U, V, and W) with six air-core coils.

A finite-element method 3-D magnetic-field analysis was performed using the ANSYS Maxwell software (ANSYS Japan,

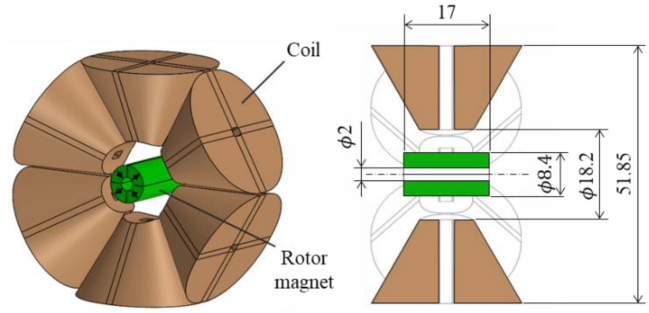

Fig. 16. Configuration and dimensions of motor.

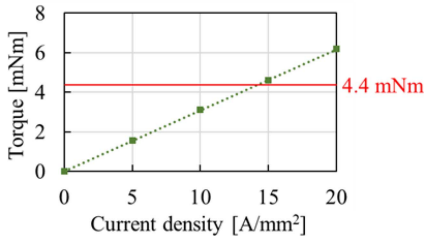

Fig. 17. Results of the generated torque by the motor with respect to the current density of the motor coils.

Tokyo). The material of the rotor was a neodymium magnet N35EH with a residual flux density of 1200 mT and coercivity of 868 kA/m. The material of the coil corresponded to copper. Current I was determined from the current density and cross-sectional area of the coil. Current I was applied to phase U and current $-I/\sqrt{2}$ was applied to phases V and W. By changing the electrical angle of the current, the maximum torque was calculated for each current density. It should be noted that the coil occupancy was set as 60% in this calculation.

During the design process, the coil outer diameter was gradually increased to achieve the target torque. As a result, the dimensions, as shown in Fig. 16, were adopted. Fig. 17 shows the simulation results of the motor torque with respect to the current density. The results show that a target value of 4.4 mN·m can be realized with a current of 14.2 A/mm^2. This coil size is too large for application to a blood pump, and the current density requires air cooling for continuous operation. Nevertheless, this design was adopted in this study to demonstrate a new levitation principle. The motor coil is air cooled by a small USB fan. The large size and high current density were caused by the use of an air-core coil and the large gap between the coil and the permanent magnet due to the impeller blades. Since the magnetic circuit allows negative stiffness in the axial direction, it is possible to propose coil size and current density for future blood pumps by applying, for example, an axial-gap motor with an iron core.

VI. Experimental Evaluation of Axial Force

A. Overview of the Experimental Device

To validate the CFD and magnetic-field analyses, we experimentally measured the axial force. Fig. 18 shows the configuration of the pump used for validation. The thrust force generated

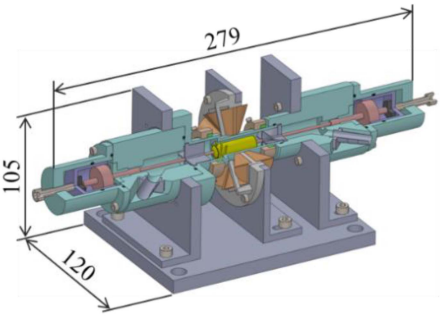

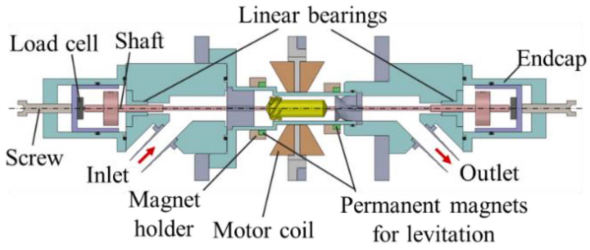

Fig. 18. Configuration of the experimental device.

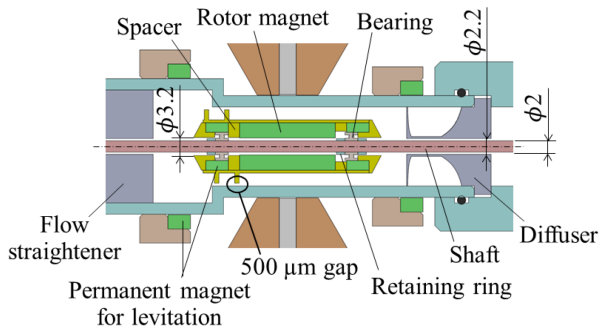

Fig. 19. Cross section of the impeller.

on the impeller can be transmitted to load cells (LMA-A-50N, Kyowa Electronic Instruments Co., Ltd., Tokyo) via a shaft that supports the impeller. It should be noted that two bearings are installed inside the impeller, as shown in Fig. 19. Hence, the shaft was not rotated. The shaft was supported by linear bearings, and the position of the impeller was adjusted by turning the screws on both ends of the experimental apparatus. The smallest gap between the impeller and housing was 500 μm. Fig. 20 shows photographs of the experimental apparatus and the components in its flow channel.

B. Measurement of Axial Thrust Force

Fig. 21 shows the mock-circulation loop used for the thrust measurement. The output of the load cell was amplified using an amplifier (WGI-470AS1, Kyowa Electronic Instruments Co., Ltd., Tokyo, Japan) and recorded using an oscilloscope (PicoScope 5442D, Pico Technology Co., Ltd., U.K.). The axial position of the impeller was measured using a laser-displacement meter (LK-G150; Keyence Co., Ltd., Tokyo). The output of the laser-displacement meter was amplified using an amplifier (LK-G3000V, Keyence Co., Ltd., Tokyo, Japan) and recorded using an oscilloscope. Pressure gauges (GP-M001, Keyence Co.,

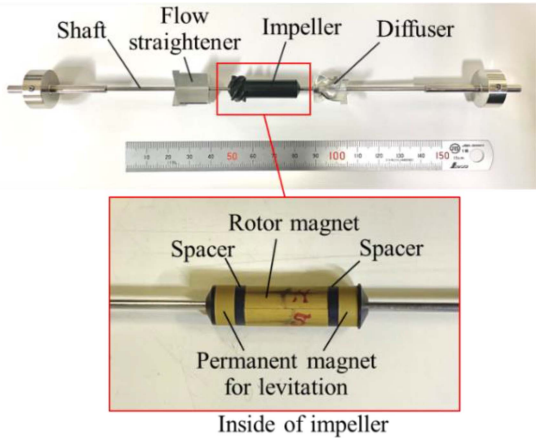

Fig. 20. Photographs of the impeller, flow straightener, and diffuser.

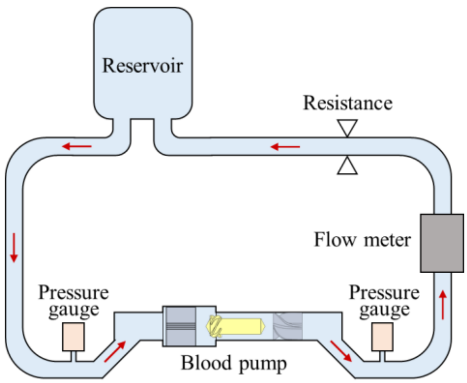

Fig. 21. Mock-circulation loop to survey motor performance.

Ltd., Tokyo, Japan) were installed at the inlet and outlet of the pump. Water and pig blood were used as the working fluids. After the impeller was set in the desired position, the measured values of the load cells by the magnetic force and screw pressurization were reset to zero. Then, the impeller was rotated to measure the thrust. The pump was operated at a flow rate of 1.5 L/min and rotational speeds of 5000, 7500, and 10 000 r/min. Fig. 22 shows a photograph of the thrust measurement when blood was used as the working fluid.

Fig. 23 shows the experimental results when water was used as the working fluid. The stiffness was calculated as the slope of the least-squares linear approximation of the thrust force at $1.5 \leq z_{\mathrm{imp}} \leq 2.5$ mm. The flow rate was set as 1.5 L/min, but the maximum flow rates were 1.1 L/min and 1.3 L/min at $z_{\mathrm{imp}} = 1.5$ mm and 2.0 mm, respectively, at 5000 r/min to ensure that the thrust at those times was recorded. At other positions and speeds, the flow rate was set to 1.5 L/min. The results indicate that the stiffness of the thrust was positive.

Fig. 24 shows the experimental results when blood was used as the working fluid. The hematocrit of the blood was measured three times using an automatic hemocytometer (MEK-6550, Nihon Kohden Co., Ltd., Tokyo), and they were 36.9%, 37.1%, and 37.2%. The viscosity of the blood was measured with a viscometer (SV-10, A&D Co., Ltd., Tokyo), and it was 5.12 mPa·s

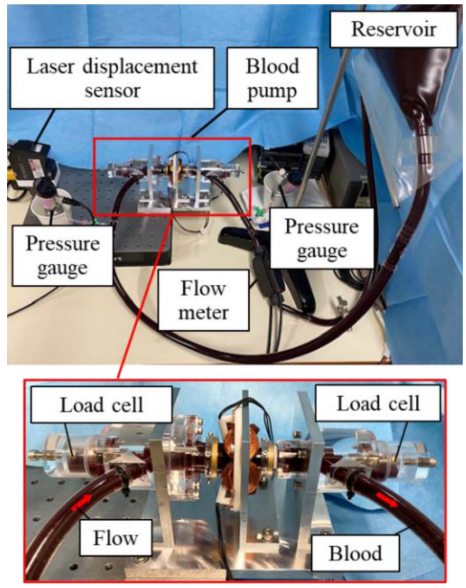

Fig. 22. Photograph of thrust measurement with blood.

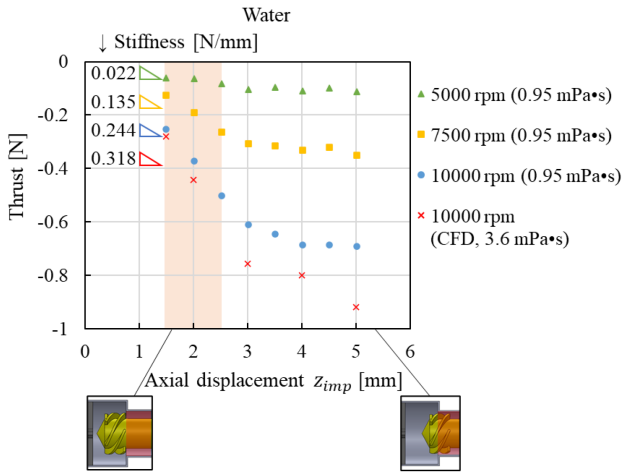

Fig. 23. Experimental results of thrust measurement in water at a flow rate of 1.5 L/min.

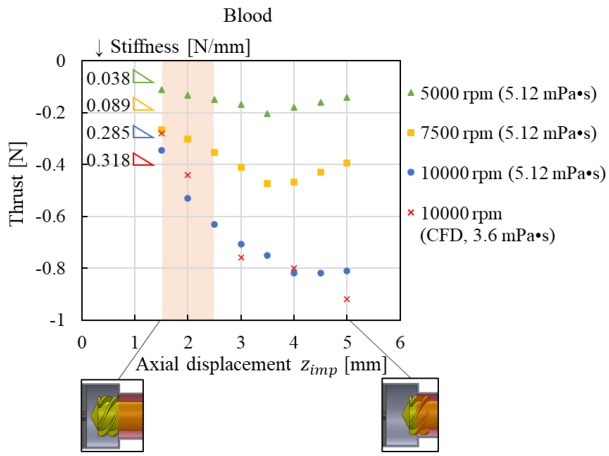

Fig. 24. Experimental results of thrust measurement in blood at a flow rate of 1.5 L/min.

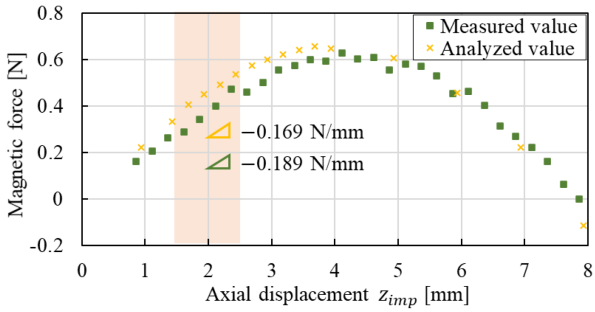

Fig. 25. Experimental results of measurement magnetic force in the axial direction.

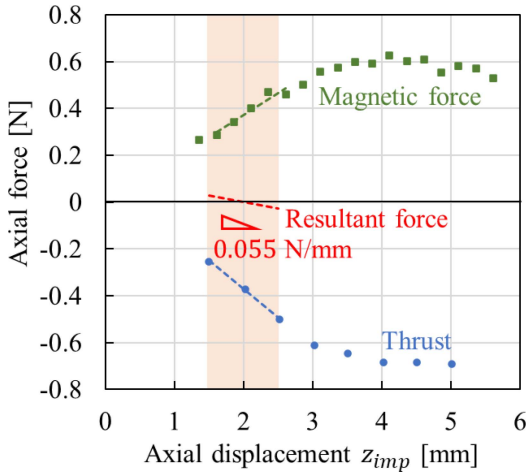

Fig. 26. Resultant force obtained from the measured magnetic force and thrust in water at 10 000 r/min and 1.5 L/min.

(21.9 °C). Although the blood viscosity was not identical to the value set by the CFD analysis due to individual differences, the experiment was conducted to evaluate whether the tendency to obtain positive stiffness with displacement was the same. The flow rate at 5000 r/min did not reach the target flow rate of 1.5 L/min, and the thrust at maximum flow was recorded. The flow rates were 0.72 L/min, 0.89 L/min, 0.98 L/min, 1.1 L/min, 1.2 L/min, 1.2 L/min, 1.3 L/min, and 1.2 L/min at $z_{\mathrm{imp}} = 1.5$ mm, 2.0 mm, 2.5 mm, 3.0 mm, 3.5 mm, 4.0 mm, 4.5 mm, and 5.0 mm, respectively. At other speeds, the flow rate was set as 1.5 L/min. The results showed that, as in the case of water, the stiffness of the thrust was positive. The tendency to obtain positive stiffness with axial displacement in the experiments and the CFD analysis was consistent.

C. Measurement of Axial Magnetic Force

Similar to the thrust measurement, the axial magnetic force was measured using load cells. Impeller displacement was measured using a laser-displacement meter. Thrust was measured without rotating the impeller. Fig. 25 shows the measured magnetic force. At $1.5 \leq z_{\mathrm{imp}} \leq 2.5$ mm, the stiffness of the measured magnetic force was −0.189 N/mm and the error against finite element method (FEM) analysis was 12%. Fig. 26 shows the resultant force calculated from the measured thrust (water, 10 000 r/min) and magnetic force. The resultant force

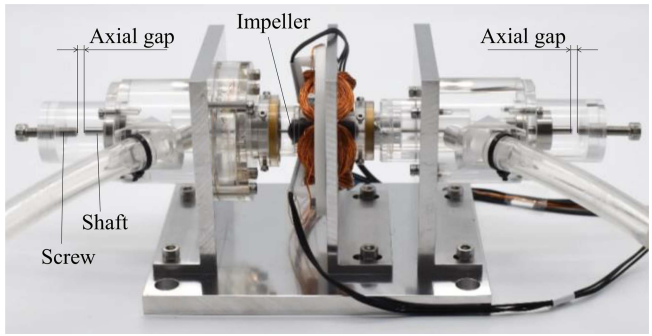

Fig. 27. Photograph of the experimental device to verify levitation in the axial direction.

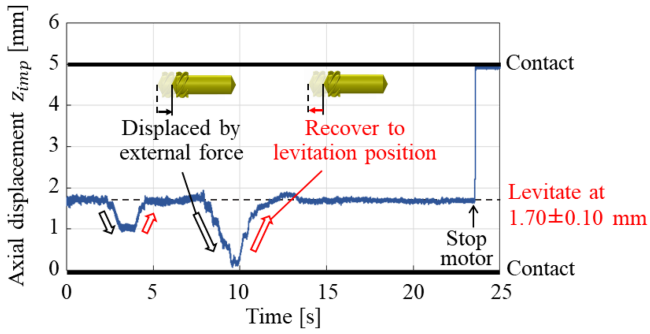

Fig. 28. Result of levitation verification in the axial direction. The pump was operated at 10 000 r/min and 1.5 L/min in water.

had a positive stiffness of 0.055 N/mm, which was 35% of that calculated by simulation. This was due to errors in the magnetic force and thrust, respectively. However, stiffness was positive and the equilibrium point existed at $z_{\mathrm{imp}} = 2.0$ mm. Therefore, it is considered to satisfy the axial levitation condition and can levitate in the axial direction.

VII. Verification of Axial Levitation

A. Evaluation of Levitation Stability

We experimentally verified axial levitation. As shown in Fig. 27, load cells were eliminated from the pump used in Section VI. The impeller is supported by a shaft in the radial and angular directions. The impeller can be displaced in the axial direction by loosening the screws at both ends of the experimental machine. The mock-circulation loop, as shown in Fig. 21, was used. The axial displacement of the impeller was measured using a laser-displacement meter. The laser output was recorded using an oscilloscope via an amplifier with a sampling period of 5 kHz. Water was used as the working fluid.

As a result of the experiment, it was determined that the impeller levitated in the axial direction. Fig. 28 shows the measured axial displacements. The lines drawn at $z_{\mathrm{imp}} = 0$ and 5 mm in the graph indicate the positions of the impeller (both ends of the shaft) contacts. At approximately 3 and 7 s, the impeller was pushed using a screw installed at the end of the pump to verify the stability of the levitation. The impeller returned to the levitation position after the displacement. The center position of the levitation was at $z_{\mathrm{imp}} = 1.70$ mm with an amplitude of

0.10 mm. Note, however, that the vibration may be suppressed by the damping effect of the linear bearing, so the shaft must be eliminated for a precise evaluation of the vibration amplitude. The pump head in the levitation position was 33.8 mmHg. When the motor was stopped at approximately 23 s, the impeller lost thrust and stopped levitation. It should be noted that the levitation was achieved in the initial permanent magnet position. However, levitation failed when the impeller was displaced significantly. Hence, the position of the external magnet on the inlet side was shifted 1 mm toward the inlet side in this experiment. Therefore, the levitation position of the impeller differed from $z_{\mathrm{imp}} = 2.0$ mm calculated in Section VI. From the experiments in Section VI and the results of the magnetic-field analysis, it is assumed that the magnitudes of the negative stiffness in the axial direction and the positive stiffness in the radial and tilt directions are reduced by about 30% each, as a result of this change in magnet position.

The results of this section show that the impeller levitated in the axial direction with the smallest gap of 500 μm without any active control.

B. Relationship Between Operating Conditions and Levitation Position

In Section VII-A, axial levitation was shown at 10 000 r/min and a flow rate of 1.5 L/min. In this section, we investigated as to how the axial levitation position changes when the rotational speed and flow rate are varied, and we evaluate the flow rate and speed range over which the impeller can levitate axially. The mock-circulation loop, as shown in Fig. 21, was used, and water was used as the working fluid. The experiments were conducted as follows. First, the impeller was rotated with the flow rate set to zero by the crump resistance. The axial displacement and pump head were recorded, while the clump was gradually loosened, and the flow rate was continuously varied from 0 to the maximum.

In this levitation system, the axial magnetic force should exhibit negative stiffness because the radial and angular directions are supported only by the magnetic force. The measured magnetic force, as shown in Fig. 25, indicates that the magnetic force exhibits a negative stiffness when $z_{\mathrm{imp}} \leq 4$ mm. Therefore, in this experiment, the screws at both ends of the experimental pump were adjusted such that the movable range of the impeller was $0 \leq z_{\mathrm{imp}} \leq 4$ mm, where the magnetic force exhibited negative stiffness. The flow rate, displacement, and pump head were recorded using an oscilloscope at a sampling frequency of 1 kHz, and the moving averages of ten interval data were calculated.

Fig. 29 shows the measured axial displacements. The lines drawn at $z_{\mathrm{imp}} = 0$ and 4 mm on the graph denote the positions where the impellers (both ends of the shaft) are in contact. The results show the relationship between the operating conditions and levitation position.

1) When the rotational speed was constant, the levitation position moved downstream as the flow rate increased.
2) When the flow rate was constant, the levitation position moved upstream as the rotational speed increased.

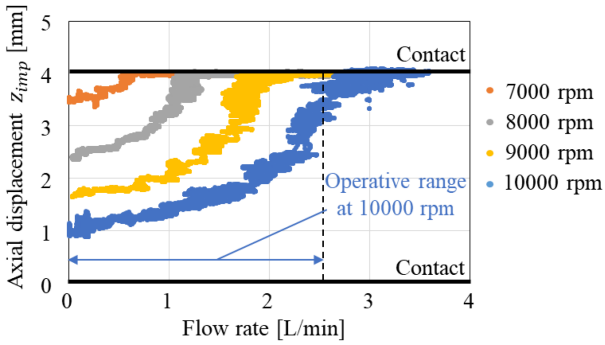

Fig. 29. Experimental results of a survey of levitation position with respect to the flow rate and rotational speed of the impeller.

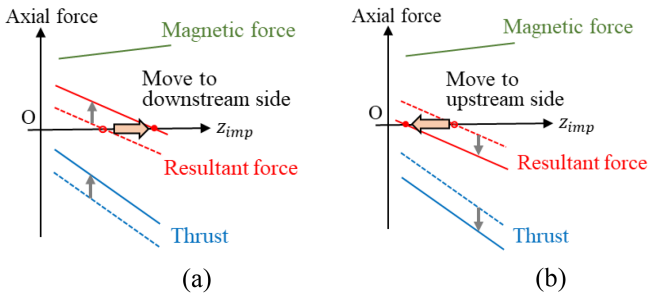

Fig. 30. Relationship between thrust and levitation position. (a) When thrust decreases. (b) When thrust increases.

Reasons for 1) are as follows. When the flow rate was increased, the resistance of the mock loop decreased because of the loosening of the crump resistance. If the rotational speed is constant, then the load on the impeller decreases as the mock loop resistance decreases. Therefore, the thrust acting on the impeller as a reaction force against blood flow generation was also reduced. As the thrust decreases, the graph of the resultant force shifts upward, as shown in Fig. 30(a), and the axial equilibrium point moves downstream. Given these reasons, when the flow rate is increased at a constant speed, the levitation position moves downstream. The reasons for 2) are as follows. As the rotational speed increases, the thrust increases. As the thrust increases, the point of equilibrium between the thrust and magnetic force moves upstream, as shown in Fig. 30(b). Therefore, when the rotational speed was increased at a constant flow rate, the levitation position moved upstream.

Furthermore, based on the results in Fig. 29, we evaluated the range of flow rates over which the axial levitation is possible. For example, at 10 000 r/min, the impeller levitated at $z_{\mathrm{imp}} = 1$ mm at a flow rate of 0 L/min. As the flow rate increased, the displacement z_{imp} also increased (moved downstream) and contact occurred when the flow rate exceeded 2.5 L/min. This confirms that the flow rate range in which levitation is possible at 10 000 r/min is from 0 to 2.5 L/min. As the rotational speed decreased, the range of the flow rate that can be levitated became narrower. Furthermore, below 6000 r/min, no levitation occurred in the range of $0 \leq z_{\mathrm{imp}} \leq 4$ mm.

Fig. 31 shows the measured pump head. The arrows in the graphs indicate the range of flow rates that can be axially

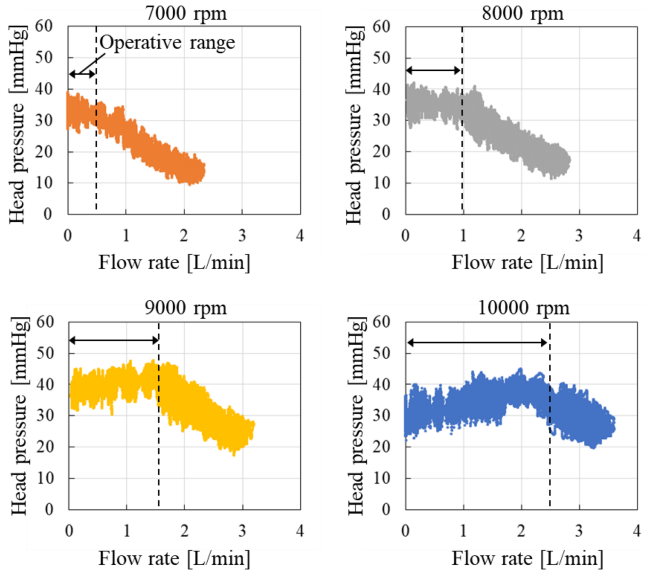

Fig. 31. Measured head pressure with respect to the flow rate and rotational speed of the impeller.

levitated. The results show that the pump head was almost constant even when the flow rate was varied within the range of levitation. Although the pump head generally decreases with increasing flow rate in the blood pumps, this trend was not observed in the levitation range of this pump. This is potentially because the pump efficiency varies with the flow rate. In this pump, as shown in Fig. 29, the position of the impeller moves upstream toward a smaller housing diameter as the flow rate increases. As the impeller blades enter a smaller channel diameter, the fluid in the pump is more likely to be drawn downstream, where the channel diameter is smaller, and the fluid is less likely to impinge on the diameter-changing area of the housing. Therefore, as the flow rate increased, the impeller moved upstream, and the pump efficiency was considered to increase.

VIII. Conclusion

In this study, thrust force levitation technology was developed to realize VADs with large gaps without an active control system. The axial magnetic force and thrust acting on the impeller were experimentally measured, and the results showed the same trend as in the simulation results. The stiffness of the resultant axial force was 0.055 N/mm. Axial levitation verification showed that the impeller levitated in the axial direction with the smallest gap of 500 μm without any active control. Furthermore, the ranges of flow rates and rotational speeds over which axial levitation was possible were clarified. The verification of levitation, including the radial and angular directions, will be examined in a future study. Although we have proposed a mechanism that achieves positive stiffness in all axial, radial, and tilt directions, it is not large enough for application to an artificial heart that includes the possibility of patients walking and falling. In a future study, we will also include optimizing the housing, impeller shape, and magnetic circuit to increase the positive stiffness.

References

[1] J. A. Cowger, "Addressing the growing U.S. donor heart shortage: Waiting for Godot or a transplant?," *J. Amer. College Cardiol.*, vol. 69, no. 13, pp. 1715–1717, Apr. 2017, doi: 10.1016/j.jacc.2017.02.010.

[2] R. Hetzer et al., "Mechanical cardiac support in the young with the Berlin heart EXCOR pulsatile ventricular assist device: 15 years' experience," *Seminars Thoracic Cardiovasc. Surg., Pediatr. Cardiac Surg. Annu.*, vol. 9, no. 1, pp. 99–108, Jan. 2006, doi: 10.1053/j.pcsu.2006.02.012.

[3] W. Hijikata et al., "A magnetically levitated centrifugal blood pump with a simple-structured disposable pump head," *Artif. Organs*, vol. 32, no. 7, pp. 531–540, Jul. 2008, doi: 10.1111/j.1525-1594.2008.00576.x.

[4] W. Hijikata et al., "Disposable Maglev centrifugal blood pump utilizing a cone-shaped impeller," *Artif. Organs*, vol. 34, no. 8, pp. 669–677, Aug. 2010, doi: 10.1111/j.1525-1594.2009.00957.x.

[5] W. Hijikata, T. Mamiya, T. Shinshi, and S. Takatani, "A cost-effective extracorporeal magnetically-levitated centrifugal blood pump employing a disposable magnet-free impeller," *Proc. Inst. Mech. Engineers, H, J. Eng. Med.*, vol. 225, no. 12, pp. 1149–1157, Dec. 2011, doi: 10.1177/0954411911422842.

[6] K. Kashiwa et al., "Survey of blood pump diaphragm damage in the NIPRO-ventricular assist device," *J. Artif. Organs*, vol. 15, no. 4, pp. 341–346, Dec. 2012, doi: 10.1007/s10047-012-0657-1.

[7] A. Loforte et al., "Levitronix centrimag third-generation magnetically levitated continuous flow pump as bridge to solution," *ASAIO J.*, vol. 57, no. 4, pp. 247–253, Jul. 2011, doi: 10.1097/MAT.0b013e31821f2116.

[8] O. H. Frazier et al., "Multicenter clinical evaluation of the heartmate vented electric left ventricular assist system in patients awaiting heart transplantation," *J. Thoracic Cardiovasc. Surg.*, vol. 122, no. 6, pp. 1186–1195, Dec. 2001, doi: 10.1067/mtc.2001.118274.

[9] B. Radovancevic et al., "Biventricular support with the Jarvik 2000 axial flow pump: A feasibility study," *ASAIO J.*, vol. 49, no. 5, pp. 604–607, Sep. 2003, doi: 10.1097/01.MAT.0000084109.47034.8A.

[10] T. Nishinaka et al., "The duraheart VAD, a magnetically levitated centrifugal pump: The University of Vienna bridge-to-transplant experience," *Circulation J.*, vol. 70, no. 11, pp. 1421–1425, 2006, doi: 10.1253/circj.70.1421.

[11] K. Yamazaki et al., "Evaheart: An implantable centrifugal blood pump for long-term circulatory support," *Jpn. J. Thoracic Cardiovasc. Surg.*, vol. 50, no. 11, pp. 461–465, Nov. 2002, doi: 10.1007/BF02919636.

[12] E. J. Molina et al., "The society of thoracic surgeons intermacs 2020 annual report," *Ann. Thoracic Surg.*, vol. 111, no. 3, pp. 778–792, Mar. 2021, doi: 10.1016/j.athoracsur.2020.12.038.

[13] T. Murashige and W. Hijikata, "Mechanical antithrombogenic properties by vibrational excitation of the impeller in a magnetically levitated centrifugal blood pump," *Artif. Organs*, vol. 43, no. 9, pp. 849–859, Sep. 2019, doi: 10.1111/aor.13541.

[14] W. Hijikata, T. Maruyama, T. Murashige, D. Sakota, and O. Maruyama, "Detection of thrombosis in a magnetically levitated blood pump by vibrational excitation of the impeller," *Artif. Organs*, vol. 44, no. 6, pp. 594–603, Jun. 2020, doi: 10.1111/aor.13632.

[15] N. Uriel et al., "Development of a novel echocardiography ramp test for speed optimization and diagnosis of device thrombosis in continuous-flow left ventricular assist devices: The Columbia ramp study," *J. Amer. College Cardiol.*, vol. 60, no. 18, pp. 1764–1775, Oct. 2012, doi: 10.1016/j.jacc.2012.07.052.

[16] I. Schalit et al., "Accelerometer detects pump thrombosis and thromboembolic events in an in vitro HVAD circuit," *ASAIO J.*, vol. 64, no. 5, pp. 601–609, Sep. 2018, doi: 10.1097/MAT.0000000000000699.

[17] F. Wang, Y. Zhu, H. Wang, and D. Zhao, "Design and analysis of a bearingless permanent-magnet motor for axial blood pump applications," *IEEE Access*, vol. 8, pp. 7622–7627, 2020, doi: 10.1109/ACCESS.2019.2959633.

[18] T. Yamane et al., "Hemocompatibility of a hydrodynamic levitation centrifugal blood pump," *J. Artif. Organs*, vol. 10, no. 2, pp. 71–76, Jun. 2007, doi: 10.1007/s10047-006-0370-z.

[19] H. Wang, Z. Wu, K. Liu, J. Wei, and H. Hu, "Modeling and control strategies of a novel axial hybrid magnetic bearing for flywheel energy storage system," *IEEE ASME Trans. Mechatron.*, vol. 27, no. 5, pp. 3819–3829, Oct. 2022, doi: 10.1109/TMECH.2022.3145705.

[20] S. Xu, J. Sun, and H. Ren, "An active magnetic bearing with controllable permanent-magnet bias field," *IEEE/ASME Trans. Mechatron.*, vol. 27, no. 5, pp. 3474–3481, Oct. 2022, doi: 10.1109/TMECH.2022.3142517.

[21] M. Hutterer and M. Schroedl, "Stabilization of active magnetic bearing systems in the case of defective sensors," *IEEE/ASME Trans. Mechatron.*, vol. 27, no. 5, pp. 3672–3682, Oct. 2022, doi: 10.1109/TMECH.2021.3131224.
[22] J. Li, G. Liu, S. Zheng, P. Cui, and Q. Chen, "Micro-jitter control of magnetically suspended control moment gyro using adaptive LMS algorithm," *IEEE/ASME Trans. Mechatron.*, vol. 27, no. 1, pp. 327–335, Feb. 2022, doi: 10.1109/TMECH.2021.3063722.
[23] S. Zheng and C. Wang, "Rotor balancing for magnetically levitated TMPs integrated with vibration self-sensing of magnetic bearings," *IEEE/ASME Trans. Mechatron.*, vol. 26, no. 6, pp. 3031–3039, Dec. 2021, doi: 10.1109/TMECH.2021.3051372.
[24] Y. Okada et al., "Mixed flow artificial heart pump with axial self-bearing motor," *IEEE/ASME Trans. Mechatron.*, vol. 10, no. 6, pp. 658–665, Dec. 2005, doi: 10.1109/TMECH.2005.859827.
[25] N. Fukushima et al., "Assessment of safety and effectiveness of the extracorporeal continuous-flow ventricular assist device (BR16010) use as a bridge-to-decision therapy for severe heart failure or refractory cardiogenic shock: Study protocol for single-arm non-randomized, uncontrolled, and investigator-initiated clinical trial," *Cardiovasc. Drugs Ther.*, vol. 32, no. 4, pp. 373–379, Aug. 2018, doi: 10.1007/s10557-018-6796-8.
[26] S. Earnshaw, "On the nature of the molecular forces which regulate the constitution of the luminferous ether," *Trans. Cambridge Philos. Soc.*, vol. 7, no. 1, pp. 97–112, 1848.
[27] K. Bourque et al., "HeartMate III: Pump design for a centrifugal LVAD with a magnetically levitated rotor," *ASAIO J.*, vol. 47, no. 4, pp. 401–405, Jul. 2001, doi: 10.1097/00002480-200107000-00020.
[28] M. Goldowsky, "Magnevad—The world's smallest magnetic-bearing turbo pump," *Artif. Organs*, vol. 28, no. 10, pp. 945–952, Oct. 2004, doi: 10.1111/j.1525-1594.2004.07386.x.
[29] H. Hoshi et al., "Magnetically suspended centrifugal blood pump with a radial magnetic driver," *ASAIO J.*, vol. 51, no. 1, pp. 60–64, Jan. 2005, doi: 10.1097/01.MAT.0000151148.72891.55.
[30] R. Hetzer et al., "First experiences with a novel magnetically suspended axial flow left ventricular assist device," *Eur. J. Cardiothoracic Surg.*, vol. 25, no. 6, pp. 964–970, Jun. 2004, doi: 10.1016/j.ejcts.2004.02.038.
[31] M. Oshima, "Flow and axial thrust through an axial pump impeller," *Turbo Machinery*, vol. 4, no. 2, pp. 102–109, 1976, doi: 10.11458/tsj1973.4.102.
[32] H. Horiguchi, S. Matsumoto, Y. Tsujimoto, M. Sakagami, and S. Tanaka, "Effect of internal flow in symmetric and asymmetric micro regenerative pump impellers on their pressure performance," *Trans. Jpn. Soc. Mech. Eng. B*, vol. 74, no. 737, pp. 121–128, 2008, doi: 10.1299/kikaib.74.121.

Ryota Magari received the B.E. degree in mechanical engineering in 2020 from the Tokyo Institute of Technology, Tokyo, Japan, where he is currently working toward the M.S. degree in mechanical engineering.

His research interests include levitation system for ventricular assist device and blood pump design.

Wataru Hijikata (Member, IEEE) received the Dr. Eng. degree in mechanical engineering from the Tokyo Institute of Technology, Tokyo, Japan, in 2010.

In 2011, he joined Toyota Central R&D Labs., Inc. In 2014, he joined Precision and Intelligence Laboratory, Tokyo Institute of Technology, as an Assistant Professor. Since 2015, he has been an Associate Professor with the Department of Mechanical Engineering, Tokyo Institute of Technology.